

Non-thermal radio emission from O-type stars

II. HD 167971

R. Blomme¹, M. De Becker², M.C. Runacres³, S. Van Loo⁴, and D. Y. A. Setia Gunawan⁵

¹ Royal Observatory of Belgium, Ringlaan 3, B-1180 Brussel, Belgium

² Institut d'Astrophysique, Université de Liège, Allée du 6 Août, 17, Bât B5c, B-4000 Liège (Sart-Tilman), Belgium

³ Vrije Universiteit Brussel, Pleinlaan 2, B-1050 Brussel, Belgium

⁴ School of Physics and Astronomy, The University of Leeds, Woodhouse Lane, Leeds LS2 9JT, UK

⁵ Australia Telescope National Facility, PO Box 76, Epping, NSW 2121, Australia

Received date / accepted date

ABSTRACT

HD 167971 is a triple system consisting of a 3.3-day eclipsing binary (O5–8 V + O5–8 V) and an O8 supergiant. It is also a well known non-thermal radio emitter. We observed the radio emission of HD 167971 with the Very Large Array (VLA) and the Australia Telescope Compact Array (ATCA). By combining these data with VLA archive observations we constructed a radio lightcurve covering a 20-yr time-range. We searched for, but failed to find, the 3.3-day spectroscopic period of the binary in the radio data. This could be due to the absence of intrinsic synchrotron radiation at the colliding-wind region between the two components of the eclipsing binary, or due to the large amount of free-free absorption that blocks the synchrotron radiation. We are able to explain many of the observed characteristics of the radio data if the non-thermal emission is produced in a colliding-wind region between the supergiant and the combined winds of the binary. Furthermore, if the system is gravitationally bound, the orbital motion occurs over a period of ~ 20 years, or longer, as suggested by the long-term variability in the radio data. We argue that the variability is due to the free-free absorption that changes with orbital phase or may also in part be due to changes in separation, should the orbit be eccentric.

Key words. stars: individual: HD 167971 – stars: early-type – stars: mass-loss – stars: winds, outflows – radio continuum: stars – radiation mechanisms: non-thermal

1. Introduction

Radio emission from most hot stars is due to thermal free-free emission by material in their stellar winds. A significant fraction of these stars, however, also show evidence of non-thermal emission. The radio fluxes of non-thermal sources are characterized by a zero or negative spectral index¹ and a high brightness temperature.

For Wolf-Rayet stars, Dougherty & Williams (2000) showed that non-thermal emission is strongly correlated with binarity. In a binary, the stellar winds of both components collide. On either side of the surface where the wind pressures balance, shocks are formed that define the extent of the colliding-wind region (Eichler & Usov 1993). Around these shocks, relativistic electrons are accelerated by the first-order Fermi mechanism (Bell 1978). These relativistic electrons then spiral in a magnetic field and thereby emit synchrotron radiation, which we detect as non-thermal radiation.

For O stars, the link between non-thermal emission and binarity was, until recently, less clear. There are a number of spectroscopically single O stars that are non-thermal emitters. In a single star, relativistic electrons could be accelerated in shocks that are due to the instability of the radiative driving mechanism (e.g. Owocki et al. 1988). However, Van Loo et al. (2006) showed that this embedded shock model cannot explain the observed spectral

index. They conclude that, just as for the Wolf-Rayet stars, all O-star non-thermal emitters should be binaries. Non-thermal emitters that are apparently single must therefore be binaries with an unfavourable inclination angle or a long-period orbit, making spectroscopic detection of their binary nature difficult. An example of such an object is HD 168112, which we studied in a previous paper (Blomme et al. 2005, hereafter Paper I). The periodic nature of the non-thermal radio fluxes suggests that this spectroscopically single star is in fact a binary, with a period estimated to be 1.4 yr.

Problems remain, however, in understanding the observed radio emission in these colliding-wind binaries. Cyg OB2 No. 5, for example, is a 6.6-day period binary where a colliding-wind region is clearly seen (in high-resolution VLA observations) between the binary and a third star. The radio flux of the binary alternates between a “high” flux state and a “low” flux state and it does so on a time-scale of ~ 7 years, rather than the 6.6-day orbital period (Miralles et al. 1994, Contreras et al. 1997). To improve our understanding of the radio emission in binaries, a more detailed study of this type of object is therefore warranted.

In this paper we study the non-thermal radio emitter HD 167971 (RA = 18^h18^m05^s.895, Dec = $-12^{\circ}14'33''.31$, J2000). Leitherer et al. (1987) found that this system consists of a 3.3213-day period eclipsing binary and a third companion. The binary components are very similar to one another in mass and temperature, but the spectral types are not well determined: they can only be constrained to the range O5–O8. From the absolute magnitudes, Leitherer et al. tentatively estimate both components to be main sequence. From a more detailed modelling

Send offprint requests to: R. Blomme,
e-mail: Ronny.Blomme@oma.be

¹ The radio spectral index α describes the power-law behaviour of the flux: $F_{\nu} \propto \nu^{\alpha} \propto \lambda^{-\alpha}$.

of the lightcurve, Davidge & Forbes (1988) propose a giant or supergiant classification. The spectral lines also show the third component to be a more luminous star, probably an O8 supergiant, and it is not known if it is gravitationally bound to the system or is just a line-of-sight object. No high spatial resolution observations are available, so the angular separation between the binary and the third component is not known. Further orbital parameters of the binary are not well determined: the eccentricity is probably $e \approx 0$. No detailed coverage of radial velocities as a function of phase in the binary orbit is available, but spectra taken near quadrature indicate a velocity amplitude of $\sim 300 \text{ km s}^{-1}$. No significant velocity variations in the spectral lines of the third component have been detected. The distance to HD 167971 can be derived from its membership of the open cluster NGC 6604, which is part of the Ser OB2 association. From the distance modulus listed by Humphreys (1978) a distance of 2 kpc is found.

The purpose of this paper is to study the colliding-wind regions in the HD 167971 system, by combining new radio observations with archive data. We construct a simple model that gives a plausible explanation for the important features seen in the radio fluxes and that is also compatible with the X-ray and VLBI (Very Long Baseline Interferometry) observations. Detailed models, such as those developed by Dougherty et al. (2003) and Pittard et al. (2006) are not used here. Many of the orbital and stellar parameters are not known (especially for the interaction between the binary and the supergiant), making the parameter space too large for sophisticated modelling.

The rest of this paper is structured as follows. In Sect. 2 we present the radio observations, with the details of the data reduction split off to Appendix A. We discuss the variability detected in the radio in Sect. 3. The observations are interpreted in Sect. 4 and the conclusions are drawn in Sect. 5.

2. Data

We observed HD 167971 with the NRAO Very Large Array² (VLA) on 2002 March 24 (at 3.6, 6 and 20 cm) and 2002 September 11 (at 3.6, 6, 18 and 20 cm). All observations were centred near HD 167971, except the 2002 September 11 observations at 18 and 20 cm, which were centred near HD 168112. The field covered at these wavelengths is large enough to contain HD 167971 as well. All observations consist of a single run on the target, preceded and followed by a phase calibrator. The details of the reduction are given in Appendix A.

In Paper I we described the Australia Telescope Compact Array³ (ATCA) observations which were collected on 2001 October 11, centred on HD 168112. The 13 and 20 cm observations have a field that is large enough to contain HD 167971. Table A.1 gives more information about the reduction of this dataset and the fluxes we determined.

We supplemented our own observations with archive data. The VLA archive contains a number of observations that are centred on, or close to, HD 167971. (The ATCA archive was also searched, but no additional data were found.) Many of these observations have not been published previously. To avoid introducing systematic effects in the data reduction, we re-reduced all

² The National Radio Astronomy Observatory is a facility of the National Science Foundation operated under cooperative agreement by Associated Universities, Inc.

³ The Australia Telescope Compact Array is part of the Australia Telescope which is funded by the Commonwealth of Australia for operation as a National Facility managed by CSIRO.

observations consistently. Details of the reduction and the measured fluxes are given in Appendix A. The 2, 3.6, 6 and 20 cm fluxes are plotted in Fig. 1.

Fig. 1 confirms the non-thermal nature of the radio emission from HD 167971. The fluxes increase with larger wavelength (with some exceptions at 20 cm) and the spectral index is therefore negative. The fluxes are also clearly variable and very high compared to what would be expected from thermal free-free emission. The stellar wind of the O8 supergiant dominates the free-free emission, with a thermal flux of only 0.1 mJy at 6 cm based on typical wind parameters listed in Table 1a.

3. Variability

3.1. Possible instrumental effects

A number of problems arose during the data reduction (see Appendix A). One of those was that many observations have a phase calibrator at a rather large angular distance from the target ($9\text{--}11^\circ$), which forced us to apply self-calibration to almost all observations. It is therefore important to check that the variability seen in Fig. 1 is not instrumental. First of all, the HD 167971 flux should not be correlated with the flux derived for the phase calibrator. The phase calibrator fluxes were determined from the AIPS task `GETJY` (except for the ATCA data, where we measured them on an image) and are listed in Table A.1. We checked those calibrators that were used in three or more observations and found that the phase calibrator and the HD 167971 flux are not significantly correlated.

Secondly, any flux changes of other targets on the same image should not be correlated with the flux changes of HD 167971. This test could only be applied at 6 cm (one other target) and 20 cm (three other targets). Again, when we tested this, no significant correlation was found. Furthermore, the range in variability in HD 167971 is substantially larger than that seen in the other targets.

The VLA instrument can be used in a number of configurations that correspond to different spatial resolutions. We therefore also need to check that the higher resolution observations do not partly resolve the target and therefore result in a lower flux. From VLBI observations, Phillips & Titus (1990) found that the linear size of the non-thermal region is at most 16 milli-arcsec (mas) at the time of their observation, which is well within the beamsize of the VLA (~ 0.5 at 6 cm, in the highest resolution configuration). Furthermore, at 6 cm, the highest-resolution A configuration gives both the highest flux value and a very low one (see Table A.1). At 20 cm, the A configuration gives the highest value, while the low values were obtained rather with the lower-resolution C configuration. The observed variability can therefore not be ascribed to our partly resolving HD 167971.

3.2. Long-term variability

It is quite obvious from Fig. 1 that the fluxes show long-term variability. This is most clearly seen at 6 and 20 cm. The 6 cm fluxes vary between ~ 8 and ~ 18 mJy (or even higher, if we include the less reliable AC216 and AD219 observations) and the 20 cm fluxes vary between ~ 4 and ~ 25 mJy (over a time-scale of 5–10 years).

The 6 cm dataset is the most complete, in the sense that it covers the ~ 20 -yr time-range reasonably well. Judging by eye, a sine function seems quite appropriate to fit the long-term trend in these data (although this is based in part on the 1988 AC216 and AD219 observations, which have large error bars). Fitting

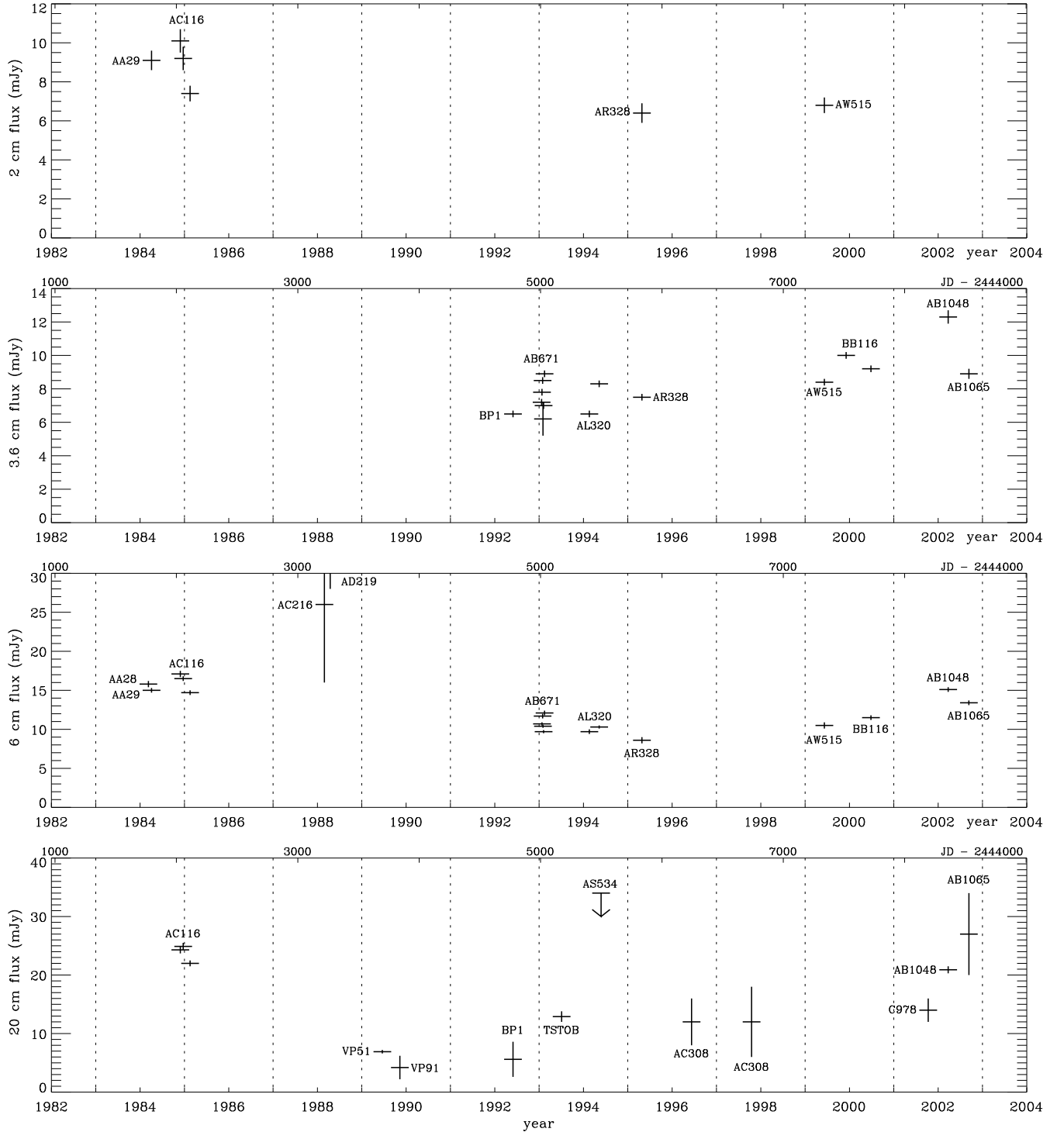


Fig. 1. The 2, 3.6, 6 and 20 cm radio fluxes of HD 167971, plotted as a function of time. Not all 20 cm upper limits are included in this figure, only those which are lower than 40 mJy. Fluxes at 0.7, 1.3, 13 and 90 cm are not plotted, because only one or two data points are available. Note that there are differences of a few percent in wavelength for observations we classed in the same band (these differences are up to 20 % in the 20 cm band). Observations are labelled by their programme name.

such a sine function, we found a ~ 20 -yr period, with a maximum around 1986.2. Of course, a period that is so similar to the time-range covered by the observations is not really convincing: much longer periods could fit the data equally well. In that case one would have to assume that the fluxes are higher outside the time-range covered.

The 20 cm data cannot be fitted with a 20-yr period sine function. Either a much longer period would be needed, or the data do not follow a sine curve. From other colliding-wind binaries, such as WR 140 (Dougherty et al. 2005), we know that the flux variation at larger wavelengths does indeed show a sharper peak than at smaller wavelengths (see Sect. 4.1). The behaviour of the

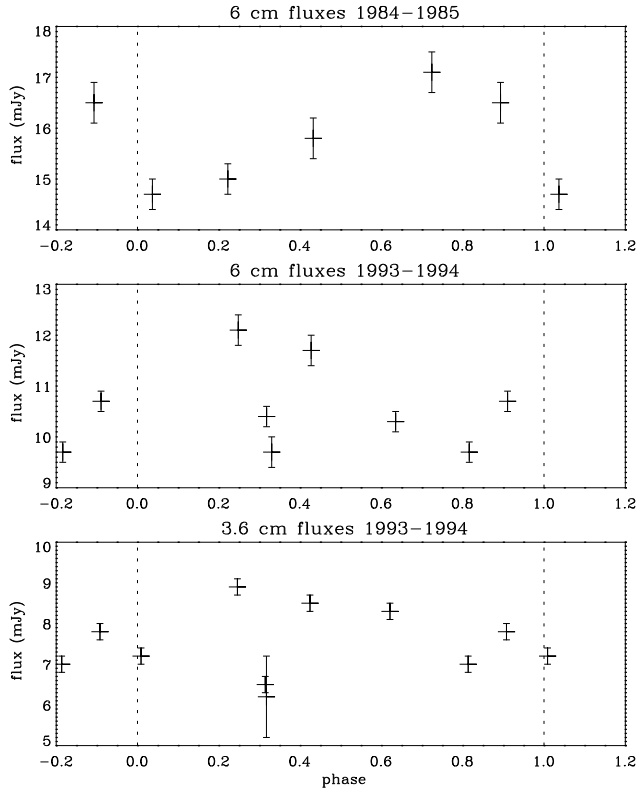


Fig. 2. Various subsets of radio observations are plotted as a function of orbital phase, with a period of $P = 3.3213$ days.

HD 167971 20 cm fluxes seems consistent with this and therefore does not contradict a 20-yr period.

The 2 and 3.6 cm fluxes show some variability, but the range is small compared to the 6 and 20 cm range. The time coverage at 2 and 3.6 cm is not as good as for 6 cm, but is still good enough to suggest that this smaller variability is real and is not due to the limited sampling.

The spectral index between 2 (or 3.6) and 6 cm is always negative, and remains between -0.3 and -0.6 most of the time. The 6–20 cm index is quite variable: it is -0.3 around 1985, is positive around 1990 (if we rely on the sine interpolation of the 6 cm data), is ~ 0.0 in 1993–1994 and is -0.3 again in ~ 2002 – 2003 . At certain times during the cycle (e.g. 1990–1994), the fluxes therefore no longer follow a power law, but show a turnover (from negative to positive spectral index) between 6 and 20 cm.

3.3. Short-term variability

Superimposed on the long-term variability, there is also shorter-term variability with a smaller amplitude. Clear examples of this are seen in the 6 cm 1984–1985 observations (projects AA28, AA29 and AC116) and the 3.6 and 6 cm 1993–1994 observations (projects AB671 and AL320). We will consider these two intervals separately: this has the advantage that we do not need to de-trend our data for the long-term variations. An important question that will be addressed is whether we can detect the 3.3-day period of the eclipsing binary in these data.

We first of all note that these short-term variations are significant. This is most easily seen by determining the χ^2 from fitting a constant to the observations. We find a reduced χ^2 of 10.8 (1984–1985), 19.6 (1993–1994, 3.6 cm) and 14.0 (1993–1994, 6 cm).

The error bars used in this calculation are from Table A.1. They cover not only the root-mean-square (RMS) noise in the map, but also include the uncertainty in the absolute flux calibration and an estimate of some of the systematic errors (see Paper I). For observations with the smallest error bars, it is the absolute flux calibration that dominates.

Fig. 2 shows that the 1984–1985 6 cm data show good orbital phase locking, suggesting that they indeed follow the 3.3-day period. However, with only 5 observations this good fit may not be very significant. A series of 100 Monte Carlo simulations in which the same fluxes were attributed random phases showed that about 30 % of those showed good phase locking (as judged by eye).

For the 1993–1994 observations, neither the 3.6 nor 6 cm fluxes show good phase locking. Especially around phase 0.2–0.4 there is a large variation in flux, which is not compatible with the expected simple behaviour of the fluxes with orbital phase. If one would presume some of the observations around phase 0.2–0.4 to be in error and eliminate them, a further problem would arise: the phase of minimum flux would then shift considerably (by ~ 0.2) between the 1984–1985 and the (remaining) 1993–1994 observations. To verify if such a phase shift is possible, we checked the optical data from the Long-term Photometry of Variables campaign (LTPV – Manfroid et al. 1991, Sterken et al. 1993) and from Hipparcos (ESA 1997). These data cover the time-range 1985–1993 and show a period that is slightly different from the Leitherer et al. (1987) one: we find 3.32157 days instead of 3.3213. This new value is closer to more recent determinations of the photometric period (3.321609 d, Mayer et al. 1992; 3.321634 d, Van Leeuwen & Van Genderen 1997). Using even the most different periods (3.321634 d vs. 3.3213 d) results in a phase shift of only 0.1 over 9 years. This is too small to explain the required phase shift between the 1984–1985 and 1993–1994 data.

In summary, we conclude that the 3.3-day period of the eclipsing binary is not detected in the radio data.

We also searched for other periods in the data. We de-trended the 3.6 and 6 cm observations by subtracting the best-fit sine curve with a 20-yr period. We then systematically tried periods between 3.3 d and 20 yr and evaluated the goodness of phase locking with the minimum string-length method (Dworetzky 1983). The most promising solutions were evaluated by eye, but no period was found that gave good phase locking for both the 3.6 and 6 cm data (in all cases, at least one data point was significantly discrepant).

4. Interpretation

4.1. Colliding-wind region inside the binary

Here, we consider the possible colliding-wind region inside the binary. Because both binary components are of equal spectral type (Leitherer et al. 1987), the collision will occur at the mid-plane between the two stars, i.e. at $21 R_{\odot}$ for an O5 V + O5 V binary (see Table 1a). If this colliding-wind region has an important contribution to the total flux, the 3.3-day binary period may be detectable in the fluxes.

We did not find the 3.3-day period in the observations, however. Two possible explanations can be suggested for this: either there is little or no intrinsic synchrotron emission, or there is too much free-free absorption for the synchrotron emission to escape. A lack of intrinsic emission could have various causes: the colliding-wind region could be too weak to provide enough energy for the synchrotron emission, the Fermi acceleration mech-

Table 1. The top panel (a) shows typical parameters for an O5 V, an O8 V and an O8 I star, based on stars of similar spectral type found in Puls et al. (1996), Repolust et al. (2004) and Markova et al. (2004). We list the radius (R_*), mass (M_*), terminal velocity (v_∞) and mass-loss rate (\dot{M}). The bottom panel (b) shows the orbital parameters, both for the inner binary and for the third component assumed to be orbiting the inner binary. In both cases, we list two possibilities for the spectral types of the inner binary components. We list the semi-major axis ($a_{1,2}$) and the amplitude of the orbital motion ($K_{1,2}$), which were calculated from the mass listed in the top panel and an assumed inclination angle of 90° . The masses of an O8 V + O8 V binary are rather low; they are not compatible with the order of $100 M_\odot$ for the total mass of the binary derived by Leitherer et al. (1987) from the observed velocity amplitude of $\sim 300 \text{ km s}^{-1}$. For the inner binary the known period was used, while for the inner binary + O8 I system, a 20-yr period was assumed.

(a) Star and wind parameters for each component				
spectral type	R_* (R_\odot)	M_* (M_\odot)	v_∞ (km s^{-1})	\dot{M} ($10^{-6} M_\odot \text{ yr}^{-1}$)
O5 V	14	45	3000	1.5
O8 V	9	13	2000	0.1
O8 I	23	50	2500	5.0

(b) Orbital parameters				
spectral type	a_1 (R_\odot)	K_1 (km s^{-1})	a_2 (R_\odot)	K_2 (km s^{-1})
Inner binary				
O5 V + O5 V	21	320	21	320
O8 V + O8 V	14	210	14	210
Triple system				
	binary		third component	
O5 V + O5 V + O8 I	2900	20	5300	37
O8 V + O8 V + O8 I	4400	31	2300	16

anism could be inefficient, or the inverse-Compton cooling could be too strong. We explore each of these possibilities in detail below.

Even for such a close binary, the velocities of the material between both components are supersonic and a colliding-wind region is formed (as X-ray observations of similar systems, such as the 3.4-day period HD 159176 confirm; De Becker et al. 2004). Radiative inhibition, however, considerably reduces the outflow velocities. Stevens & Pollock (1994) calculated the effect of radiative inhibition for a somewhat similar binary (HD 160652, O6.5 V + O6.5 V, $P = 6.14$ d). Extrapolating the results of their Fig. 4 to our even closer system, we estimate that the outflow velocity at the shock is $v \approx 500 \text{ km s}^{-1}$.

We first check that the collision between the winds is energetic enough to provide the synchrotron emission. In this order-of-magnitude analysis, we assume HD 167971 to be an O5 V + O5 V binary with star and wind parameters based on literature values for similar stars (see Table 1). The total kinetic energy of both winds is $\dot{M}v^2 = 2.4 \times 10^{35} \text{ erg s}^{-1}$. Assuming the size of the emission region is $\sim \pi r_{\text{OB}}$ (Eichler & Usov 1993), where $r_{\text{OB}} = 21R_\odot$, the fractional solid angle of the stellar winds impinging on the non-thermal emission region is ~ 0.23 , and the kinetic luminosity available to the wind-collision region is $5.5 \times 10^{34} \text{ erg s}^{-1}$. We estimate a total radio luminosity of $\sim 1.6 \times 10^{30} \text{ erg s}^{-1}$ at a distance of 2 kpc, which can easily be provided from the kinetic luminosity of the winds.

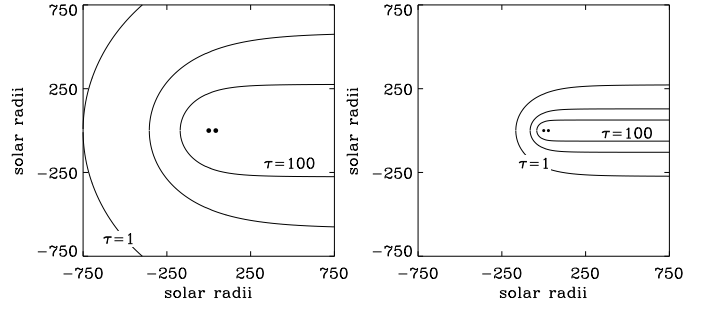


Fig. 3. Contours of optical depth at 6 cm in the stellar wind of an O5 V star (left panel) and an O8 V star (right panel). The observer is situated to the left. The contour lines of $\tau = 1, 10$ and 100 are shown. The two dots indicate the position of both components of the binary.

For the Fermi acceleration to be efficient, the Alfvén Mach number

$$M_A = \frac{v \sqrt{4\pi\rho}}{B} \quad (1)$$

should not be too small (Wentzel 1974; Jones & Ellison 1991, Sect. 4.1.1). B is the magnetic field at the shock and v and ρ are the pre-shock velocity and density. Assuming a value of $M_A = 4$ and a pre-shock density of $7.0 \times 10^{-14} \text{ g cm}^{-3}$, we find that B should be 12 G. Assuming a Weber & Davis (1967) type magnetic field structure, this leads to a surface field that is small compared to the usual assumption of a 100 G surface field (compatible with the detection limit, see Mathys 1999).

We next explore the possibility that inverse-Compton (IC) cooling is too strong because of the large supply of UV photons available in this close binary. These photons IC scatter off the relativistic electrons and thereby remove energy. The time needed for IC cooling to reduce the momentum of an electron from a high value p_c down to p can be found by integrating Eq. (6) of Van Loo et al. (2005):

$$\Delta t = \frac{3\pi m_e^2 c^3 r^2}{\rho \sigma_T L_*}, \quad (2)$$

where we assumed that $p \ll p_c$. As we typically consider radio fluxes in the 2 – 20 cm wavelength range, we determine the time required to cool down to a momentum that has maximum synchrotron emission just beyond 20 cm. Using the relation between momentum and the frequency at which the maximum flux is emitted (Van Loo et al., their Eq. (19)), we find $\Delta t \approx 600 \text{ s}$ (for an assumed $L_* = 10^6 L_\odot$). During that time, the electron has moved over a distance $v\Delta t \approx 0.5 R_\odot$.

Due to the IC cooling, the size of the synchrotron emitting region is therefore rather small. This makes it doubtful whether the colliding-wind region inside the binary can generate a significant amount of synchrotron emission. Redoing the analysis for later-type components in the binary, or (super)giants, results in a similar size for the synchrotron emitting region (within a factor of three). If the components are O5 supergiants, then we note that the Alfvén number requirement results in a $\sim 40 \text{ G}$ magnetic field at the shock, which translates into a surface field that is in better agreement with an assumed surface field of 100 G.

We finally explore the possibility that the free-free absorption is so large that all of the synchrotron emission is absorbed at all phases in the orbit. In Fig. 3, we show the contours of optical depth (τ) at 6 cm. To simplify the figure and discussion,

we consider the free-free effects of only a single star. The optical depth was calculated from the formulae given in Wright & Barlow (1975). Fig. 3 also shows the position of both components. For the purposes of this figure we have assumed that the inclination is exactly 90° (we know it is close to 90° , because it is an eclipsing binary). The size of the colliding-wind region is somewhat larger than the binary separation and all of the synchrotron radiation will be found close to this region (see above). We see on Fig. 3 that the synchrotron-emitting region is well within the $\tau = 10$ contour surface and would therefore be undetectable⁴. (If the components are both giants or supergiants (Davidge & Forbes 1988) rather than main-sequence stars, then the opacity effects discussed here will be even stronger.)

Another possibility is the intrinsic synchrotron emission from the wind-collision region in the binary is absorbed by free-free opacity of the O8 supergiant wind. However, as the relative positions of the supergiant and the binary system are unknown this remains an open question.

4.2. Colliding-wind region between the supergiant and the binary

The major part of the observed non-thermal emission of HD 167971 is not due to the colliding-wind region inside the binary, because (i) we do not detect the 3.3-day period, (ii) the intrinsic synchrotron flux is estimated to be small, and (iii) the free-free absorption is large. We can therefore conclude that the main source of the observed non-thermal radio emission must be the colliding-wind region between the O8 supergiant and the binary. We recall that from spectroscopic observations (Leitherer et al. 1987) it is not clear if the supergiant and the binary are gravitationally bound. The supergiant could be coincidentally in the same line of sight and might even be at a (somewhat) different distance. However, we will assume in our analysis that the supergiant and the eclipsing binary do form a gravitationally bound system. This allows us to attribute the long-term variability to the relative motion of the binary and the supergiant.

The orbital period is then ~ 20 years, or possibly longer (Sect. 3.2). With the typical stellar parameters for an O8 supergiant and the eclipsing binary, a 20-year period corresponds to a separation $a_1 + a_2 \geq 6700 R_\odot$ (see Table 1b), provided we assume a nearly-circular orbit. This is well beyond the $\sim 1600 R_\odot$ radius at which $\tau = 1$ for 6 cm in the supergiant wind. Most of the time we therefore see the intrinsic synchrotron emission at this wavelength.

At 20 cm, the $\tau = 1$ radius is much larger ($\sim 3500 R_\odot$). A much longer part of the orbit will therefore be spent inside the 20 cm radio photosphere (except for inclinations near 0°), explaining why the maximum at 20 cm is much more peaked. At wavelengths shorter than 6 cm, the radio photosphere is much smaller and the colliding-wind region is therefore outside the radio photosphere nearly all the time, explaining the lack of substantial variation at 2 and 3.6 cm. The observed changes in the 6–20 cm spectral index and the turnover between 6 and 20 cm during part of the period (Sect. 3.2) can thus be ascribed to these opacity effects. An alternative explanation for the turnover

would be the Razin effect. Due to this effect, the synchrotron emission deviates from a power law at longer wavelengths and the long-wavelength spectral index can become zero or even positive. The strength of the Razin effect depends on the (local) magnetic field and electron density. In an eccentric orbit, both quantities would vary with orbital phase, and therefore, so would the spectral index. More sophisticated models would be required to derive quantitative orbital information from this alternative explanation of the turnover.

Eichler & Usov (1993) made a simple model for the synchrotron radiation emitted in a colliding-wind binary. When we apply their analysis to the present data, we find an intrinsic synchrotron flux (i.e. without free-free absorption) of ~ 25 mJy at 6 cm, which is in surprisingly good agreement with the observed values. The Eichler & Usov model does contain a number of unconstrained parameters for which we adopted their default values. Hence, the agreement should only be interpreted as showing the plausibility of our model.

We next try to explain the variability of the flux and the turnover between 6 and 20 cm (which occurs during part of the orbit) by ascribing them to the changing free-free absorption due to the orbital motion of the synchrotron-emitting source and the O8 supergiant. We used a simple model, where we assumed the intrinsic synchrotron emission to come from a point source in a 20-yr circular orbit around the supergiant (with stellar parameters as in Table 1a). Simulations show that we can reproduce the 6 cm radio lightcurve quite well, provided we use a low-inclination orbit (otherwise the flux would be completely absorbed). However, free-free absorption increases considerably from 6 to 20 cm, and we cannot match the 6 and 20 cm data with the same model. This is most probably due to our assumption that the synchrotron-emitting region is a point source. In reality, the synchrotron-emitting region will be extended and deriving quantitative information about the opacity from the flux or the turnover will therefore require more sophisticated models, which are beyond the scope of this paper.

Further information on the size of the synchrotron-emitting region comes from the Phillips & Titus (1990) observations. They found a size of 16 mas, which corresponds to a diameter of $\sim 6500 R_\odot$ at 18 cm. This is comparable to the separation between the binary and the O supergiant. The size of the colliding-wind region makes it difficult to put constraints on the orbital inclination. If the inclination of the orbit is close to 90° , a point-like source of synchrotron emission would be eclipsed at 6 cm during ~ 2 years of the 20-year orbit, as it passes behind the free-free radius of the supergiant; but this is contradicted by the observations. However, for a larger-sized colliding-wind region, this argument cannot be used, as there is probably always some part of it that is not eclipsed. No constraints on the orbital inclination can therefore be derived.

The shorter-term variability could be attributed to stochastic variations due to clumping in the stellar winds, as suggested for WR 146 and WR 147 (Setia Gunawan et al. 2000, 2001). These affect the synchrotron emitting region itself (as the density and/or velocity of the material entering the colliding-wind region changes) and affect the free-free absorption. The AB671 series represents a typical example of such flux variations. The 6 cm fluxes range between 10 mJy and 12 mJy. We can derive an estimate of how much the density needs to change to explain this flux variation through additional free-free absorption. If, for simplicity, we assume the synchrotron emitting region to be a point source, we can use the Wright & Barlow (1975) formulae to determine how much optical depth has to be added to change the 12 mJy flux into 10 mJy. When the free-free opti-

⁴ One should be careful with this conclusion. In the WR 140 system, for instance, the colliding-wind region is well within the free-free radius of the Wolf-Rayet star during the whole orbit. The O star wind blows a low-density region in the Wolf-Rayet wind and it is through this region that we can see the synchrotron emission, at least part of the time (Williams et al. 1990). The winds of the HD 167971 binary are nearly equal, and therefore no such complications arise here.

cal depth along the line-of-sight is 1, a 10 % increase in density suffices. For larger-sized sources, the density contrasts will need to be considerably larger to offset the cancellations that occur in a stochastically clumped wind.

The model proposed here is also compatible with the X-ray data, studied by De Becker et al. (2005b). From *XMM-Newton* observations, they found an excess of a factor of 4, compared to the canonical L_X vs. L_{bol} relation for O stars. The emission is probably thermal and shows the presence of a high-temperature plasma component (~ 20 MK). The colliding-wind region within the eclipsing binary is unlikely to produce such high plasma temperatures as the winds of the two O5–O8 V stars collide before they reach their terminal velocities, thereby producing softer thermal X-ray emission. The high plasma temperature should therefore be ascribed to material heated in the colliding-wind region between the eclipsing binary and the O8 supergiant. The existence of this interaction shows that the supergiant must be at approximately the same distance as the binary, and is not an accidental line-of-sight object.

The two ROSAT data points plotted on Fig. 5 of De Becker et al. (2005b) show X-ray flux decreasing between 1993 and 1995. This decline closely follows the radio emission during the same period. We attribute this to the intrinsic X-ray and synchrotron emission varying in a correlated way, as they both depend on the shock strength and the absorption in the stellar wind material. However, De Becker et al. caution that the observed variability might be attributed to systematic effects between *XMM-Newton* and ROSAT data, as seen in Cyg OB2 No. 8A (De Becker et al. 2005a).

5. Conclusions

In this paper we analysed the available radio data on HD 167971 from the VLA and ATCA. The negative spectral index confirms the non-thermal nature of the radio emission. The fluxes are also very high (compared to thermal) and they are variable.

At the core of the HD 167971 triple system is a 3.3-day period eclipsing binary. No modulation of the radio fluxes with this period was detected. We can explain this by a rather low intrinsic synchrotron flux (due to a low acceleration efficiency and/or strong inverse-Compton cooling), or by the large amount of free-free absorption in the stellar wind material. We therefore conclude that most of the non-thermal emission must come from the colliding-wind region between the O8 supergiant and the combined winds of the binary.

The hypothesis that the O8 supergiant and the binary have a colliding-wind interaction provides a plausible explanation for many of the characteristics of the radio and X-ray observations. If, furthermore, the system is gravitationally bound, the observed variability can be ascribed to the orbital motion. The proposed orbital period of ~ 20 years is large enough to be well beyond the $\tau = 1$ free-free radius. Some absorption still occurs, explaining the long-term variability of the radio fluxes. The high X-ray temperature plasma component found by De Becker et al. (2005b) can also be ascribed to this colliding-wind region. The problem of fitting the 6 and 20 cm radio fluxes simultaneously with a point-source model, and the Phillips & Titus (1990) resolved observations suggest a colliding-wind region of substantial size.

While this model provides a good explanation for the observations, independent verification still needs to be sought. Verification of our HD 167971 model can most easily be obtained from high-resolution, high S/N optical spectra. These should bring definite evidence that the triple system is indeed gravitationally bound and should allow us to obtain better stellar

and orbital parameters for the binary. Once these data are available, quantitative models for the X-ray and non-thermal radio emission can be developed.

Acknowledgements. We are grateful to the referee, Sean Dougherty, for his helpful and constructive comments. We also thank Joan Vandekerckhove for his help with the reduction of the VLA data and the original observers of the data we used from the VLA archive. We are grateful to Jan Cuypers, Herman Hensberge, Julian Pittard and Gregor Rauw for useful discussions. This research has made use of the SIMBAD database, operated at CDS, Strasbourg, France and NASA's Astrophysics Data System Abstract Service. Part of this research was carried out in the framework of the project IUAP P5/36 financed by the Belgian Science Policy Office.

Appendix A: Data reduction

The data reduction was done using the Astronomical Image Processing System (AIPS), developed by the NRAO. The different reduction steps consist of assigning the standard fluxes to the flux calibrators, calibration, imaging and cleaning. These steps have been described in detail in the Appendix to Paper I. On some observations made with low spatial resolution, Galactic background structure can be seen. This background can easily be filtered out by using the properties of the Fourier transform that is an essential part of radio interferometry: we simply drop those visibilities that were measured on the shortest baselines and thereby eliminate the large-scale background structure. In doing so, we took care not to remove more data than strictly needed. Technical information on the reduction is listed in Table A.1.

In a considerable number of cases, the distance of the phase calibrator to HD 167971 is large ($9\text{--}11^\circ$, see Table A.1). The antenna gains could therefore be significantly different between the phase calibrator and target scans. We therefore systematically applied selfcalibration to those observations that have detections. We did one round of phase-only selfcalibration (a second round does not make any significant difference). For the time-interval over which to integrate, we took the shortest time-interval that gave smooth phase solutions (phase scatter of less than $\sim 20^\circ$): this is usually 3 or 5 min. Observations with phase scatter significantly larger than 20° have been listed in the “notes” column to Table A.1. No selfcalibration was applied to the AC308 observations (because of their short on-target time) and the ATCA data.

On the selfcalibrated images, the fluxes were measured by fitting an elliptical Gaussian to the source. We checked that the resulting fluxes are in good agreement with the maximum intensity (this is consistent with HD 167971 being a point source on all our images). The fluxes are listed in Table A.1. The necessity for using selfcalibration is clearly shown by a number of observations that have substantially larger fluxes for HD 167971 on the selfcalibrated images than on the non-selfcalibrated images. The largest effect is seen in the AB671 (1993-02-01) 3.6 cm observation, where the selfcalibrated flux is 6.2 ± 1 mJy, while the non-selfcalibrated one is only 2.6 mJy.

The error bars listed in this table cover not only the root-mean-square (RMS) noise in the map, but also include the uncertainty in the absolute flux calibration (2 % for the 3.6, 6, 20 and 90 cm observations and 5 % for the other wavelengths) and an estimate of some of the *systematic* errors (see Paper I). For those observations with relatively small error bars, it is the uncertainty in the absolute flux calibration that dominates. In those cases where HD 167971 is off-centre, its flux was corrected for primary beam attenuation and beamwidth smearing.

For the observations where HD 167971 was not detected, we assign an upper limit of 3 times the RMS, where the RMS

is measured in a small box around the source. If the source is off-centre, this upper limit is corrected for the primary beam attenuation and beamwidth smearing. A number of 20 cm observations containing HD 167971 are of such low quality that they do not even provide a significant upper limit: BAUD (1980-07-12 and 1982-02-28), FIX (1982-05-22) and AT143 (1993-06-11). A number of 90 cm observations were also rejected for the same reason.

In some 20 cm observations HD 167971 is within the primary beam on two images centred on different targets. In that case we only list the one closest to HD 167971 because this gives the smallest error bar. In most cases the flux of the other image is compatible with the flux listed. The exceptions are: AC116 (1984-DEC-21), where the off-centre measurement of HD 167971 is a factor of two lower than the on-centre measurement and BP1, where the off-centre value is a factor of two higher than the on-centre value. A smaller effect is seen for VP51, where the off-centre value is 30 % higher than the on-centre value. Simulations show that the effect in the high-resolution AC116 observation is due to noise in the map. For the low-resolution BP1 and VP51, we checked that decreasing the background even further (by throwing away more short baselines) leads to a much better agreement. Some caution must therefore be used in off-centre fluxes, such as the low-resolution AC308 observations. (Note that the values listed for AC116, BP1 and VP51 in Table A.1 do not suffer from this problem because they are based on the on-centre measurements.)

A number of observations have used two flux calibrators. We checked that using either calibrator results in the same flux (within the error bars). This gave good agreement in most cases, except AL320 (1994-FEB-18) 3.6 cm, where there is a 32 % difference. Checking other observations made around the same time shows that the (uncalibrated) fluxes of 3C48 are anomalously low for the observation we are interested in, while the (uncalibrated) 3C286 fluxes remain the same over all the observations considered. The calibration of this observation is therefore made on 3C286. A similar problem exists for AL320 (1994-FEB-18) 6 cm. Applying the same technique shows that, in this case, 3C48 is the more reliable calibrator. We also note that for the TSTOB observation we used the flux calibrator from another programme, nearby in time (see Paper I).

The reduction of the ATCA observations C978 was detailed in Paper I. These observations are centred on HD 168112, but the 13 and 20 cm primary beams are large enough that they also contain HD 167971. Because these data were collected in a number of spectral channels, we can apply multi-frequency synthesis: this results in images that are not beamwidth smeared.

A comparison between our fluxes and those that have been published in the literature shows that our error bars are usually larger, because we include the flux calibration errors and some estimate of systematic effects. Our 2 cm determinations are systematically higher than the literature values. This is because of the improvement due to the selfcalibration reduction technique. A similar, but smaller, effect is seen at 6 cm. For the 20 cm observations of Bieging et al. (1989) we obtain lower fluxes. The VLA Calibrator Manual instructions (Perley & Taylor 2003) for this specific combination of wavelength, flux calibrator and VLA configuration show that the results obtained should be reduced by 6 %. We speculate that Bieging et al. did not apply this 6 % reduction; doing so results in an acceptable agreement between their fluxes and ours. Our upper limit to the AR328 0.7 cm observation (4.5 mJy) is much higher than the Contreras et al. (1996) value of 1.72 mJy. We note that this is a 19 min observation using only 10 antennas, which gives a theoretical RMS of

0.7 mJy/beam. The 3 sigma upper limit of 1.72 mJy claimed by Contreras et al. is therefore too optimistic, and we have greater confidence in our result.

References

- Bell, A. R. 1978, *MNRAS*, 182, 147
 Bieging, J. H., Abbott, D. C., & Churchwell, E. B. 1989, *ApJ*, 340, 518
 Blomme, R., Van Loo, S., De Becker, M., et al. 2005, *A&A*, 436, 1033 (Paper I)
 Contreras, M. E., Rodríguez, L. F., Gómez, Y., & Velázquez, A. 1996, *ApJ*, 469, 329
 Contreras, M. E., Rodríguez, L. F., Tapia, M., et al. 1997, *ApJ*, 488, L153
 Davidge, T. J., Forbes, D. 1988, *MNRAS*, 235, 797
 De Becker, M., Rauw, G., Pittard, J. M., et al. 2004, *A&A*, 416, 221
 De Becker, M., Rauw, G., & Swings, J.-P. 2005a, *Ap&SS*, 297, 291
 De Becker, M., Rauw, G., Blomme, R., et al. 2005b, *A&A*, 437, 1029
 Dougherty, S. M., & Williams, P. M. 2000, *MNRAS*, 319, 1005
 Dougherty, S. M., Pittard, J. M., Kasian, L., et al. 2003, *A&A*, 409, 217
 Dougherty, S. M., Beasley, A. J., Claussen, M. J., Zauderer, B. A., & Bolingbroke, N. J. 2005, *ApJ*, 623, 447
 Dworetzky, M. M. 1983, *MNRAS*, 203, 917
 Eichler, D., & Usov, V. 1993, *ApJ*, 402, 271
 ESA 1997, *The Hipparcos and Tycho Catalogues*, ESA SP-1200
 Humphreys, R. M. 1978, *ApJS*, 38, 309
 Jones, F. C., & Ellison, D. C. 1991, *Space Sci. Rev.* 58, 259
 Leitherer, C., Forbes, D., Gilmore, A. C., et al. 1987, *A&A*, 185, 121
 Manfroid, J., Sterken, C., Bruch, A., et al. 1991, *A&AS*, 87, 481
 Markova, N., Puls, J., Repolust, T., & Markov, H. 2004, *A&A*, 413, 693
 Mathys, G. 1999, in *Variable and Non-spherical Stellar Winds in Luminous Hot Stars*, ed. B. Wolf, O. Stahl, & A. W. Fullerton, *Lect. Notes Phys.*, 523, 95
 Mayer, P., Dreschsel, H., & Lorenz, R. 1992, *IBVS*, 3805, 1
 Miralles, M. P., Rodríguez, L. F., Tapia, M., et al. 1994, *A&A*, 282, 547
 Owocki, S. P., Castor, J. I., & Rybicki, G. B. 1988, *ApJ*, 335, 914
 Perley, R. A., & Taylor, G. B. 2003, *The VLA Calibrator Manual*
<http://www.aoc.nrao.edu/~gtaylor/calib.html>
 Phillips, R. B., & Titus, M. A. 1990, *ApJ*, 359, L15
 Pittard, J. M., Dougherty, S. M., Coker, R. F., O'Connor, E., & Bolingbroke, N. J. 2005, *A&A*, 446, 1001
 Puls, J., Kudritzki, R. P., Herrero, A., et al. 1996, *A&A*, 305, 171
 Repolust, T., Puls, J., & Herrero, A. 2004, *A&A*, 415, 349
 Setia Gunawan, D. Y. A., De Bruyn, A. G., Van der Hucht, K. A., & Williams, P. M. 2000, *A&A*, 356, 676
 Setia Gunawan, D. Y. A., De Bruyn, A. G., Van der Hucht, K. A., & Williams, P. M. 2001, *A&A*, 368, 484
 Sterken, C., Manfroid, J., Anton, K., et al. 1993, *A&AS*, 102, 79
 Stevens, I. R., & Pollock, A. M. T. 1994, *MNRAS*, 269, 226
 Van Leeuwen, F., & Van Genderen, A. M. 1997, *A&A*, 327, 1070
 Van Loo, S., Runacres, M. C., & Blomme, R. 2005, *A&A*, 433, 313
 Van Loo, S., Runacres, M. C., & Blomme, R. 2006, *A&A*, 452, 1011
 Weber, E. J., & Davis, L., Jr. 1967, *ApJ*, 148, 217
 Wentzel, D. G. 1974, *ARA&A*, 12, 71
 Williams, P. M., Van der Hucht, K. A., Pollock, A. M. T., et al. 1990, *MNRAS*, 243, 662
 Wright, A. E., & Barlow, M. J. 1975, *MNRAS*, 170, 41

Table A.1. Reduction of VLA and ATCA data. Programme C978 is an ATCA observation, all others are VLA observations. Column (1) gives the programme name, (2) the date of the observation, (3) the phase calibrator (J2000 coordinates), (4) the flux of the phase calibrator \pm the rms (in Jy), (5) the distance of HD 167971 to the phase calibrator (degrees), (6) the integration time (in minutes) on the source, (7) the number of antennas that gave a usable signal, (8) the configuration the VLA was in at the time of the observation, (9) the RMS in the centre of the image (not listed in case on an upper limit), (10) the measured flux (in mJy) and (11) refers to the notes. Many of the VLA observations were made in two sidebands, each of which has a bandwidth of 50 MHz; the exceptions are noted in column (11). Upper limits are $3 \times$ the RMS. Numbers between brackets in the notes column give references for those observations that have already been published in the literature.

(1) progr.	(2) date	(3) phase calibrator		(5) dist.	(6) intgr. time	(7) no. ants.	(8) config	(9) RMS (mJy)	(10) flux (mJy)	(11) notes
		name	flux							
0.7 cm										
AR328	1995-04-27	1733-130	11.15 \pm 0.15	11.0	19	10	D		< 4.5	(3)
1.3 cm										
AW515	1999-06-08	1832-105	1.023 \pm 0.015	3.9	50	19	AD	0.22	6.0 \pm 0.6	PH,X
2 cm										
AA29	1984-04-04	1733-130	5.69 \pm 0.09	11.0	22	24	C	0.18	9.1 \pm 0.5	(1)
AC116	1984-11-27	1733-130	7.3 \pm 0.1	11.0	28	25	A	0.16	10.1 \pm 0.6	PH,(1)
AC116	1984-12-21	1733-130	7.1 \pm 0.2	11.0	26	27	A	0.18	9.2 \pm 0.6	PH,(1)
AC116	1985-02-16	1733-130	6.56 \pm 0.06	11.0	37	25	A	0.13	7.4 \pm 0.4	PH,(1)
AR328	1995-04-27	1733-130	9.77 \pm 0.06	11.0	22	16	D	0.25	6.4 \pm 0.5	PH,(3)
AW515	1999-06-08	1832-105	1.25 \pm 0.01	3.9	30	20	AD	0.21	6.8 \pm 0.4	PH
3.6 cm										
BP1	1992-05-30	1733-130	5.00 \pm 0.03	11.0	55	24	CD	0.05	6.5 \pm 0.2	
AB671	1993-01-21	1811-209	0.179 \pm 0.001	8.8	42	22	A	0.04	7.2 \pm 0.2	X
AB671	1993-01-24	1811-209	0.186 \pm 0.003	8.8	19	27	A	0.05	7.8 \pm 0.2	X
AB671	1993-01-29	1811-209	0.175 \pm 0.001	8.8	20	26	BnA	0.05	8.5 \pm 0.2	X
AB671	1993-02-01	1811-209	0.174 \pm 0.001	8.8	7	27	BnA	0.11	6.2 \pm 1	X
AB671	1993-02-06	1811-209	0.179 \pm 0.001	8.8	19	27	BnA	0.04	7.0 \pm 0.2	X
AB671	1993-02-14	1811-209	0.188 \pm 0.001	8.8	9	27	BnA	0.10	8.9 \pm 0.2	X
AL320	1994-02-18	1733-130	4.85 \pm 0.06	11.0	12	26	AC	0.06	6.5 \pm 0.2	PH
AL320	1994-05-10	1733-130	4.69 \pm 0.05	11.0	10	24	AB	0.07	8.3 \pm 0.2	
AR328	1995-04-27	1733-130	6.74 \pm 0.02	11.0	11	16	D	0.12	7.5 \pm 0.2	X,(3)
AW515	1999-06-08	1832-105	1.36 \pm 0.01	3.9	10	20	AD	0.11	8.4 \pm 0.2	
BB116	1999-12-04	1822-096	1.37 \pm 0.02	2.8	121	19	B	0.03	10.0 \pm 0.2	X
BB116	2000-06-26	1822-096	1.340 \pm 0.003	2.8	117	26	DnC	0.03	9.2 \pm 0.2	
AB1048	2002-03-24	1832-105	1.67 \pm 0.04	3.9	8	26	A	0.07	12.3 \pm 0.4	
AB1065	2002-09-11	1832-105	1.29 \pm 0.02	3.9	7	26	CnB	0.11	8.9 \pm 0.3	
6 cm										
AA28	1984-03-09	1733-130	5.74 \pm 0.01	11.0	19	26	CnB	0.08	15.8 \pm 0.4	(1)
AA29	1984-04-04	1733-130	5.69 \pm 0.03	11.0	11	27	C	0.11	15.0 \pm 0.3	(1)
AC116	1984-11-27	1733-130	5.02 \pm 0.02	11.0	21	24	A	0.09	17.1 \pm 0.4	(1)
AC116	1984-12-21	1733-130	5.05 \pm 0.02	11.0	41	26	A	0.06	16.5 \pm 0.3	(1)
AC116	1985-02-16	1733-130	5.312 \pm 0.015	11.0	19	24	A	0.09	14.7 \pm 0.3	(1)
AC216	1988-02-27	1811-209	0.303 \pm 0.002	8.8	15	25	CnB	0.07	26 \pm 10	B,PH
AD219	1988-04-15	1804+010	1.149 \pm 0.004	13.7	17	26	CD	0.04	34 \pm 6	B,PH
AB671	1993-01-24	1811-209	0.324 \pm 0.002	8.8	19	27	A	0.05	10.7 \pm 0.2	
AB671	1993-01-29	1811-209	0.318 \pm 0.001	8.8	19	26	BnA	0.07	11.7 \pm 0.3	
AB671	1993-02-01	1811-209	0.314 \pm 0.001	8.8	13	27	BnA	0.07	10.4 \pm 0.2	
AB671	1993-02-06	1811-209	0.322 \pm 0.001	8.8	19	27	BnA	0.06	9.7 \pm 0.2	
AB671	1993-02-14	1811-209	0.319 \pm 0.001	8.8	10	27	BnA	0.08	12.1 \pm 0.3	
AL320	1994-02-18	1733-130	5.09 \pm 0.06	11.0	9	26	AC	0.09	9.7 \pm 0.3	PH
AL320	1994-05-10	1733-130	4.43 \pm 0.02	11.0	10	26	AB	0.08	10.3 \pm 0.2	
AR328	1995-04-27	1733-130	5.04 \pm 0.02	11.0	11	16	D	0.20	8.6 \pm 0.4	(3)
AW515	1999-06-08	1832-105	1.200 \pm 0.015	3.9	10	20	AD	0.16	10.5 \pm 0.4	
BB116	2000-06-26	1822-096	2.25 \pm 0.03	2.8	93	26	DnC	0.05	11.5 \pm 0.3	X
AB1048	2002-03-24	1832-105	1.32 \pm 0.01	3.9	6	26	A	0.09	15.1 \pm 0.3	
AB1065	2002-09-11	1832-105	1.26 \pm 0.07	3.9	5	26	CnB	0.14	13.4 \pm 0.3	
13 cm										
C978	2001-10-11	1832-105	1.042 \pm 0.002	3.9	120	6	EW352	0.26	11 \pm 2	B,X
20 cm										
AC116	1984-11-27	1733-130	5.55 \pm 0.03	11.0	28	25	A	0.12	24.3 \pm 0.6	PH,(1)
AC116	1984-12-21	1733-130	5.90 \pm 0.04	11.0	10	27	A	0.17	24.9 \pm 0.6	(1)
AG163	1984-12-24	1743-038	1.281 \pm 0.015	11.9	1	27	A		< 100	B,2x25
AC116	1985-02-16	1733-130	6.36 \pm 0.03	11.0	15	25	A	0.12	22.0 \pm 0.5	(1)
AB531	1989-05-01	1834-126	0.518 \pm 0.001	3.9	2	26	B		< 100	B,1x50
VP51	1989-06-19	1733-130	5.200	11.0	59	25	C	0.24	6.9 \pm 0.3	PH,X,C
AG290	1989-07-20	1833-210	13.02 \pm 0.03	9.6	0	27	CD		< 80	B
VP91	1989-11-10	1733-130	6.2 \pm 0.2	11.0	56	27	D	1.5	4.2 \pm 2	PH,X,(2)
BP1	1992-05-30	1911-201	3.0 \pm 0.2	15.0	91	25	CD	0.8	5.6 \pm 3	PH

Table A.1. continued.

(1) progr.	(2) date	(3) phase calibrator		(5) dist.	(6) intgr. time	(7) no. ants.	(8) config	(9) RMS (mJy)	(10) flux (mJy)	(11) notes
		name	flux							
TSTOB	1993-07-05	1822-096	4.3 ± 0.2	2.8	13	27	C	0.3	12.9 ± 0.9	
AS534	1994-05-21	1822-096	5.39 ± 0.04	2.8	4	21	BnA		< 70	B,1x3.125
AS534	1994-05-26	1822-096	4.99 ± 0.03	2.8	5	25	BnA		< 34	B,X,1x3.125
AS534	1994-06-01	1822-096	5.15 ± 0.02	2.8	4	25	BnA		< 150	B,X,1x3.125
AC308	1996-06-08	1833-210	10.78 ± 0.02	9.6	1	27	DnC		< 190	B
AC308	1996-06-09	1833-210	10.80 ± 0.02	9.6	1	27	DnC	2.0	12 ± 4	B
AC308	1996-06-16	1833-210	10.78 ± 0.02	9.6		27	DnC		< 70	B
AC308	1997-10-16	1833-210	10.07 ± 0.02	9.6	1	27	DnC	2.0	12 ± 6	B
C978	2001-10-11	1832-105	0.929 ± 0.001	3.9	120	6	EW352	0.42	14 ± 2	B,X
AB1048	2002-03-24	1834-126	0.534 ± 0.001	3.9	3	26	A	0.20	20.9 ± 0.6	
AB1065	2002-09-11	1834-126	0.468 ± 0.001	3.9	5	26	CnB	6	29 ± 23	B,I,18cm
AB1065	2002-09-11	1834-126	0.529 ± 0.001	3.9	5	21	CnB	3	27 ± 7	B,20cm
90 cm										
AH299	1988-06-21	1829+487	42.6 ± 0.5	61.0	47	21	DnC		< 270	B,2x3.125
AH299	1989-05-28	1829+487	41.7 ± 0.5	61.0	57	25	CnB		< 80	B,2x3.125

Notes:

- B Observation is not centred on HD 167971. The flux has been corrected for that.
No correction for beamwidth smearing needs to be applied to C978.
- C for VP51, no flux calibrator was available, so we calibrated the flux on the phase calibrator, to which we assigned the value listed in Perley & Taylor (2003).
- I Interference is high in the AB1065 18 cm image.
- PH The phases in the selfcalibration gain solutions show scatter that is significantly larger than 20° .
- X The phase calibrator is of low quality (AB671, C978), is not listed in the VLA Calibrator Manual (Perley & Taylor 2003; AW515 at 1.3 cm, BB116), or the recommended constraints on the uv-range could not be applied (AR328 at 3.6 cm).
- (1) Bieging et al. (1989).
(2) Phillips & Titus (1990).
(3) Contreras et al. (1996).

List of Objects

'HD 168112' on page 1
'Cyg OB2 No. 5' on page 1
'HD 167971' on page 1
'NGC 6604' on page 2
'Ser OB2' on page 2
'HD 159176' on page 5
'HD 160652' on page 5
'3C48' on page 8
'3C286' on page 8
'1733-130' on page 9
'1832-105' on page 9
'1811-209' on page 9
'1822-096' on page 9
'1804+010' on page 9
'1743-038' on page 9
'1834-126' on page 9
'1833-210' on page 9
'1911-201' on page 9
'1829+487' on page 10